Electronic Supporting Information

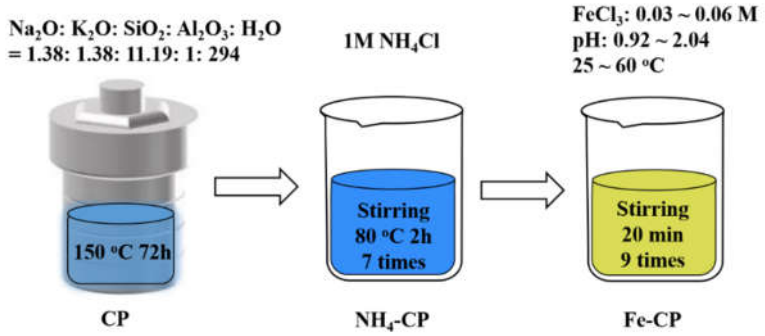

Scheme S1. Scheme 1. Schematic of the Fe-CP preparation.

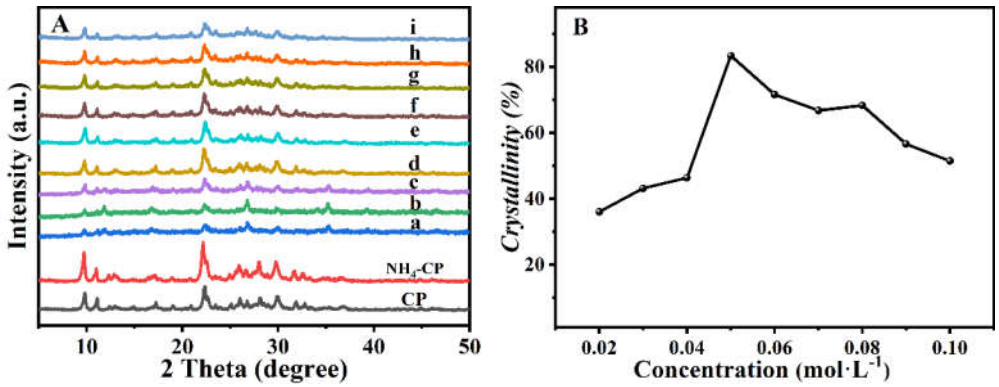

Figure S1. XRD patterns (A) and relative crystallinity of CP, NH_4-CP, and Fe(0.03)-HCl(y)-CP (B). y = 0.02 (a), 0.03 (b), 0.04 (c), 0.05 (d), 0.06 (e), 0.07 (f), 0.08 (g), 0.09 (h), and 0.10 (i).

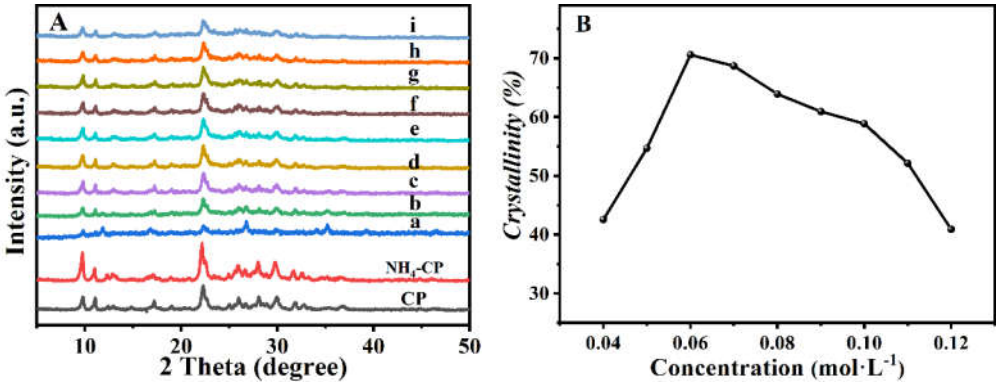

Figure S2. XRD patterns and relative crystallinity of CP, NH_4-CP, and Fe(0.06)-HCl(y)-CP. y = 0.04 (a), 0.05 (b), 0.06 (c), 0.07 (d), 0.08 (e), 0.09 (f), 0.10 (g), 0.11 (h), and 0.12 (i), respectively.

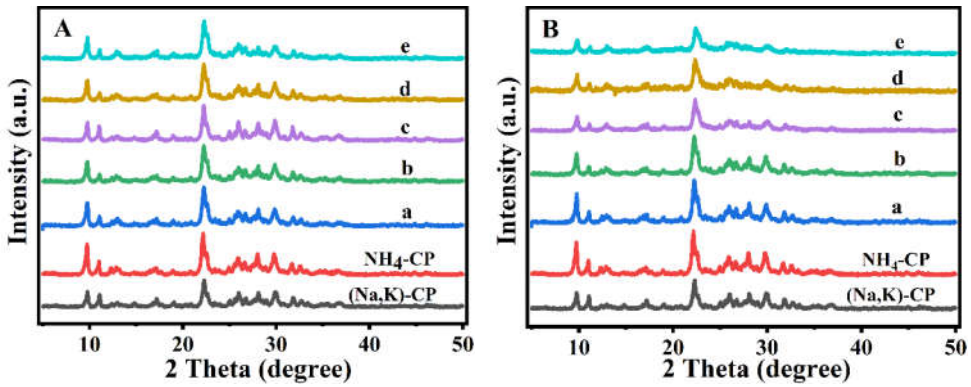

Figure S3. XRD patterns of CP, NH_4-CP, Fe(0.03)-HCl(0.05)-a-CP (A) and Fe(0.06)-HCl(0.07)-CP-a (B). a = 1 (a), 3 (b), 5 (c), 7 (d), and 9 (e), respectively.

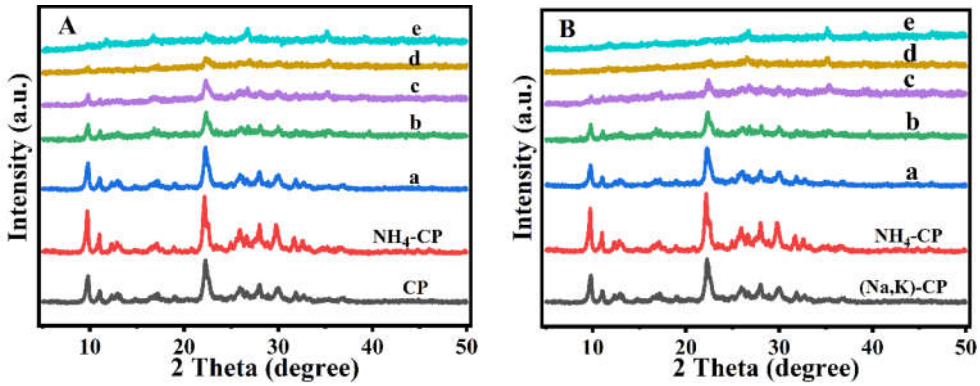

Figure S4. XRD patterns of CP, NH_4-CP, and Fe(0.03)-HCl(0.00)-CP-a (A) and Fe(0.06)-HCl(0.00)-CP-a (B). x = 1 (a), 3 (b), 5 (c), 7 (d), and 9 (e).

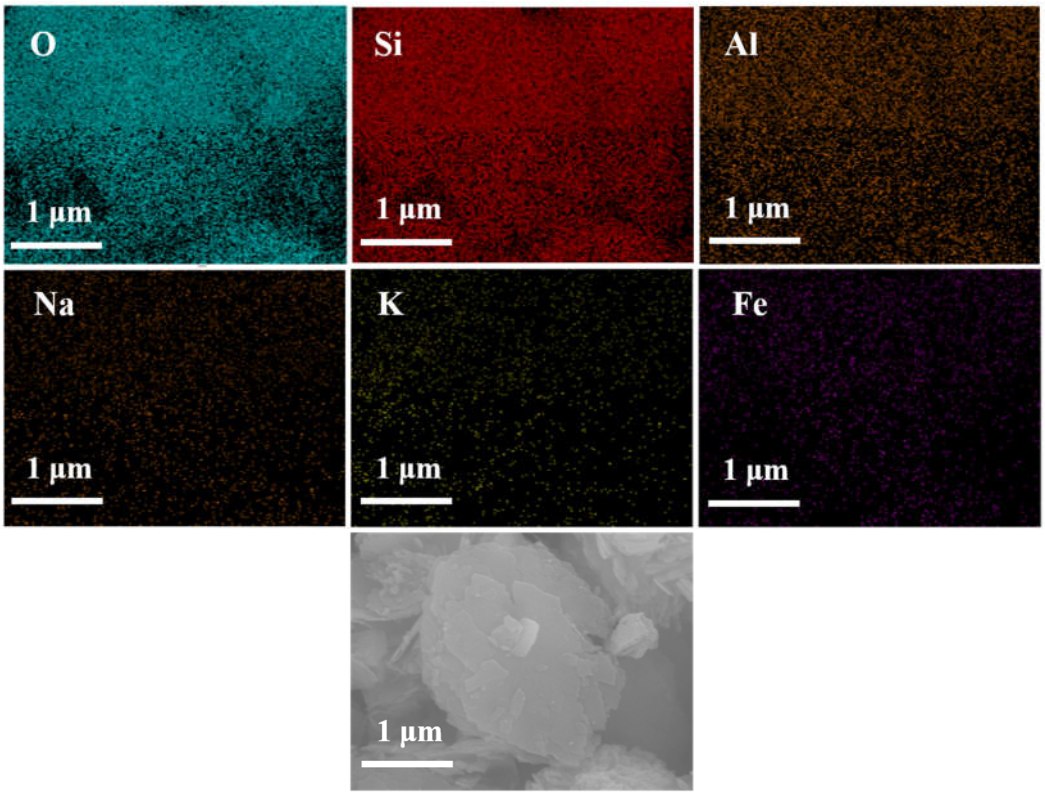

Figure S5. SEM elemental mapping of Fe(0.03)-HCl(0.00)-9-CP.

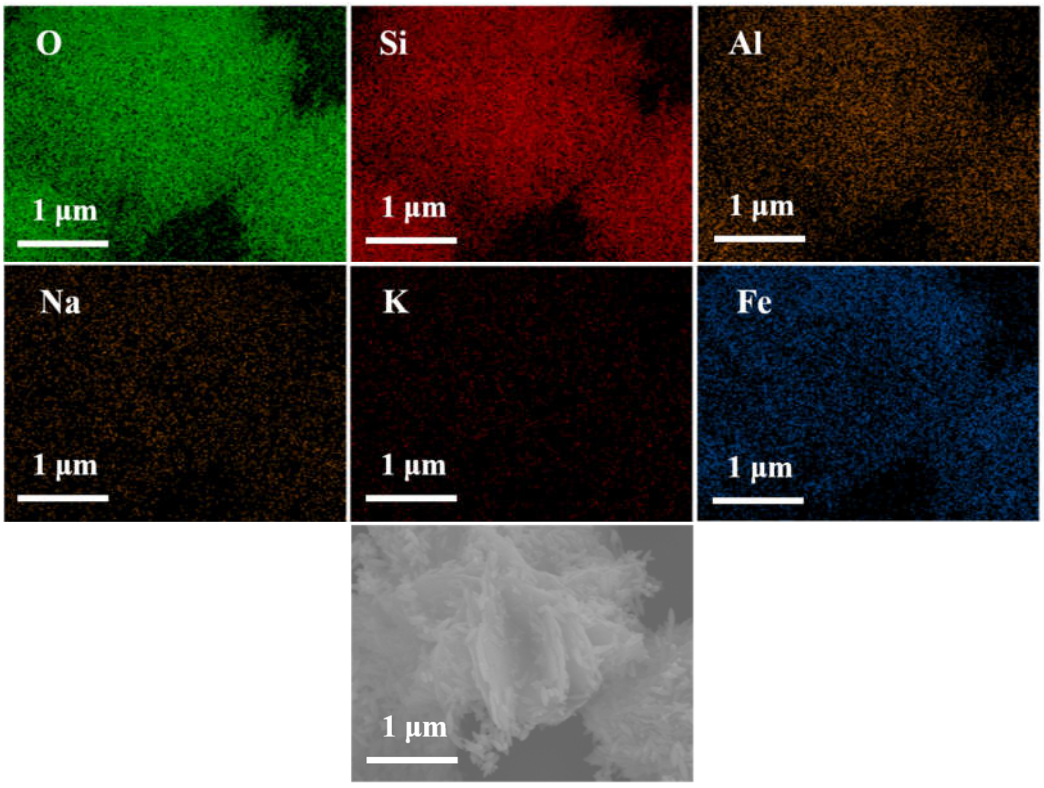

Figure S6. SEM elemental mapping of Fe(0.03)-HCl(0.05)-9-CP.

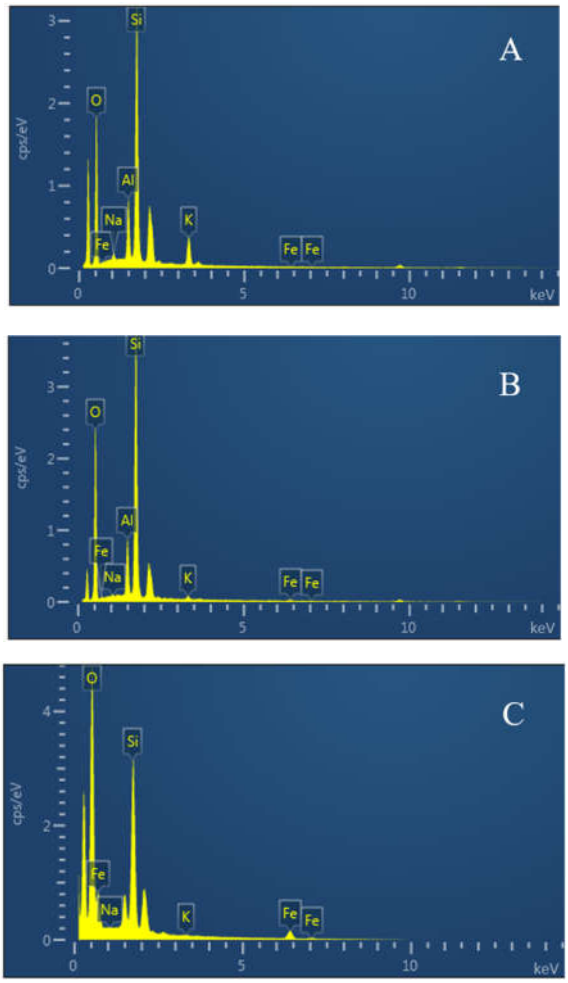

Figure S7. Energy dispersive X-ray (EDX) analysis of CP (A), Fe(0.03)-H(0.05)-CP-9 (B) and Fe(0.03)-H(0.00)-CP-9 (C).

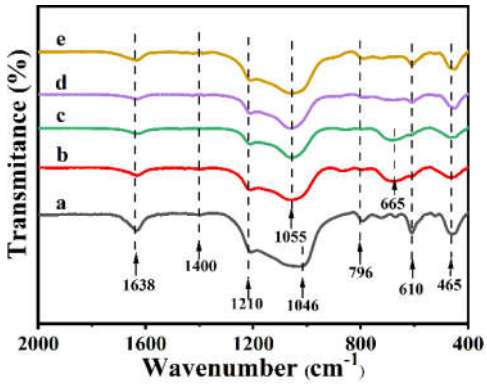

Figure S8. FT-IR spectra of various CPs. (a) CP, (b) Fe(0.03)-H(0.00)-CP-9, (c) Fe(0.06)-H(0.00)-CP-9, (d) Fe(0.03)-H(0.05)-CP-9, and (e) Fe(0.06)-H(0.07)-CP-9.

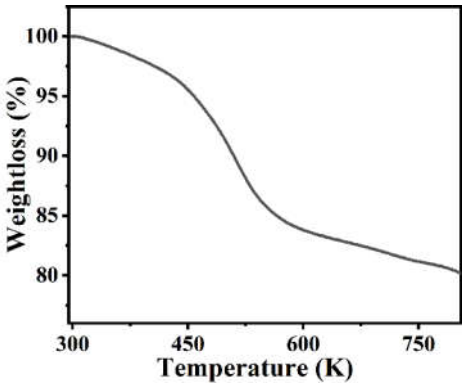

Figure S9. TG result for the bare FeOOH.

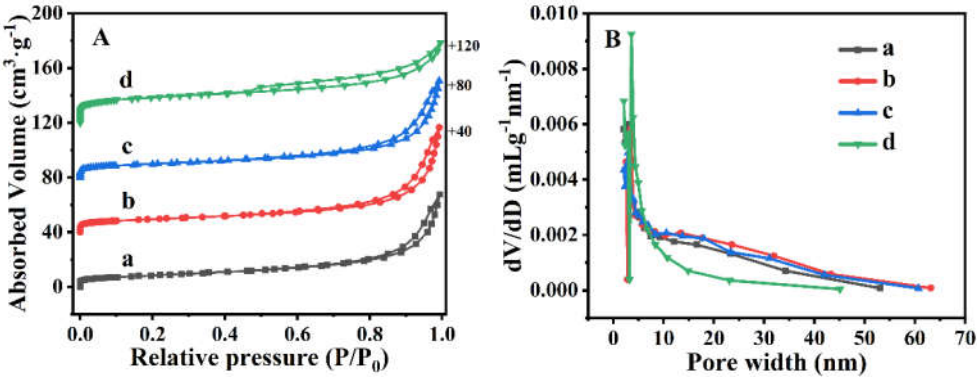

Figure S10. N_2 adsorption-desorption isotherms of (a) CP, (b) Fe(0.03)-H(0.05)-CP-3, (c) Fe(0.03)-H(0.05)-CP-9, and (d) Fe(0.03)-H(0.00)-CP-9, corresponding their mesopore size distribution (B).

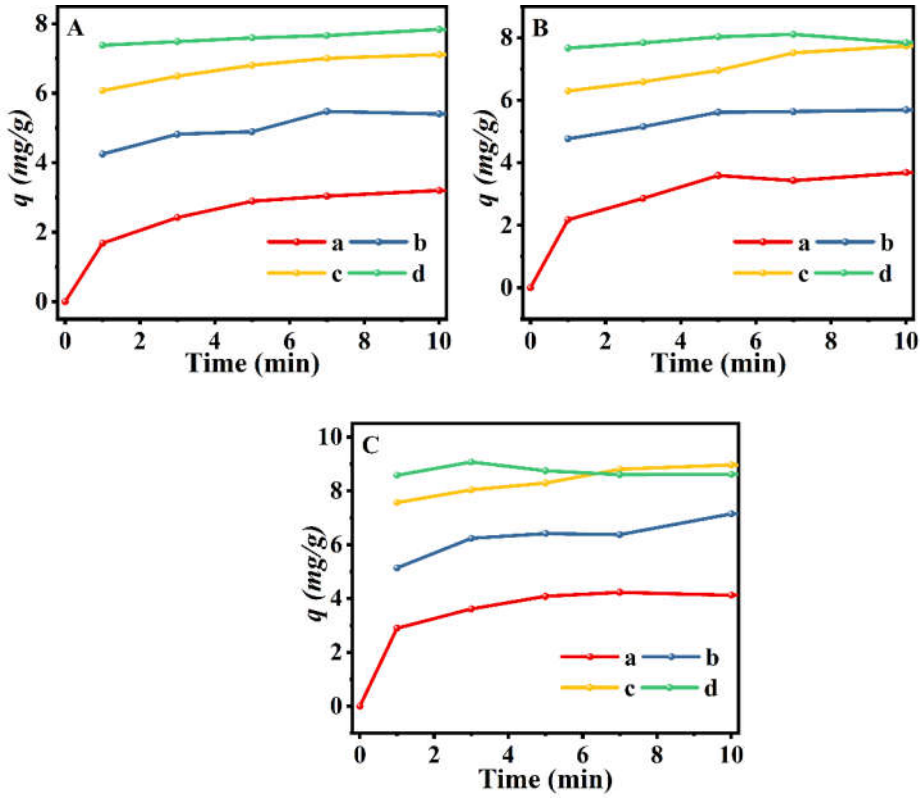

Figure S11. Kinetic curves of Fe(0.06)-H(0.07)-CP-x at 298 K (A), 313 K (B), and 333 K (C). x = 1 (a), 3 (b), 5 (c), 7 (d), and 9 (e).

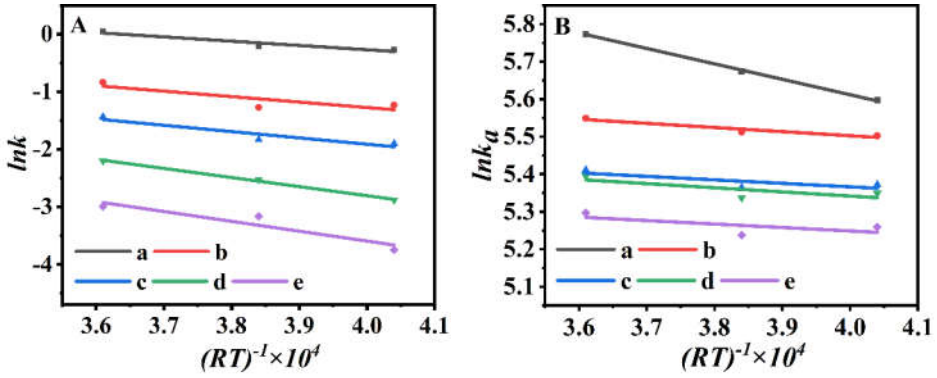

Figure S12. Relationships between *ln k* and $(RT)^{-1} \times 10^4$ (A), as well as *ln* K_a and $(RT)^{-1} \times 10^4$ (B) of Fe(0.03)-HCl(0.05)-x-CP. x = 1 (a), 3 (b), 5 (c), 7 (d), and 9 (e).

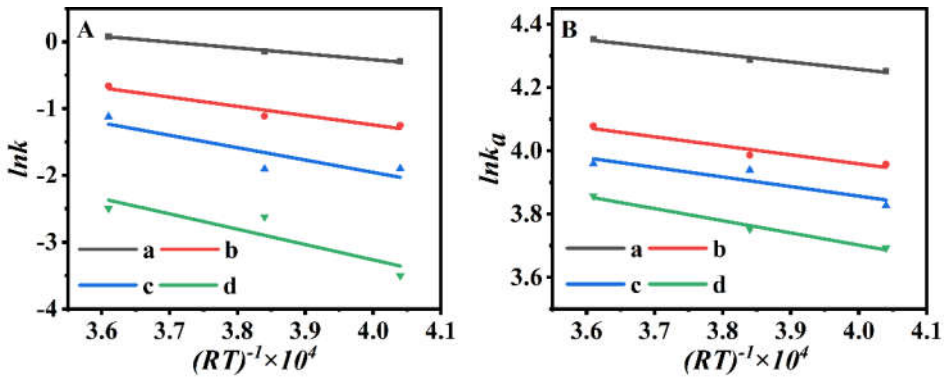

Figure S13. Relationships between *ln k* and $(RT)^{-1} \times 10^4$ (A), as well as *ln* k_a and $(RT)^{-1} \times 10^4$ (B) of Fe(0.06)-HCl(0.07)-x-CP. x = 1 (a), 3 (b), 5 (c), and 7 (d).

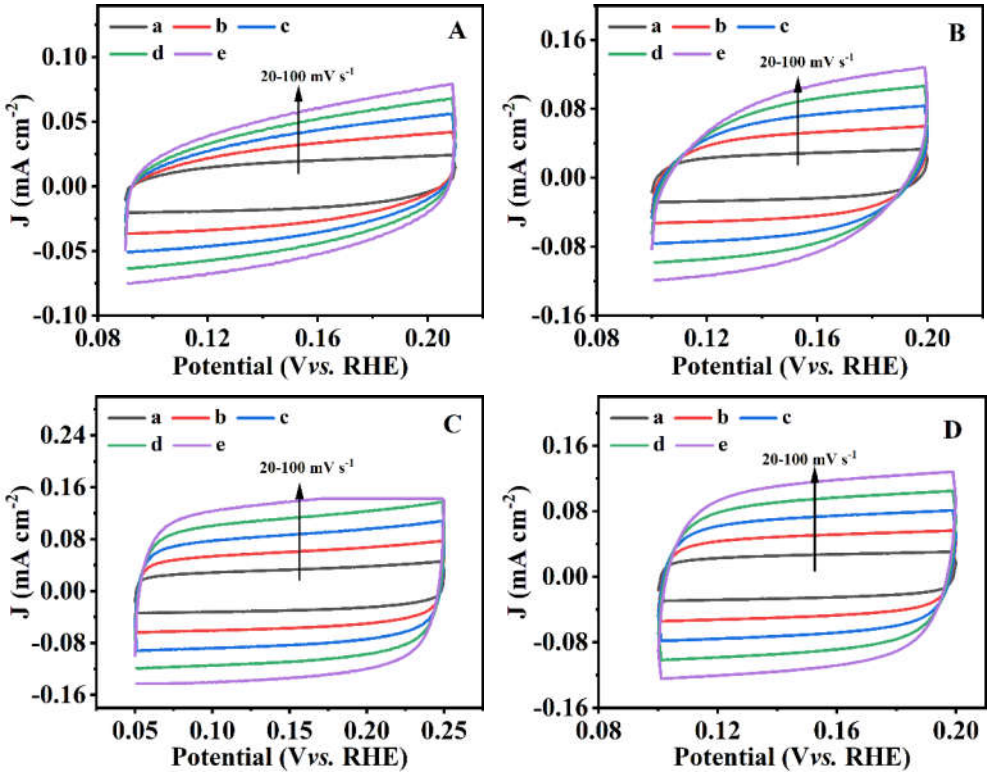

Figure S14. CV curves at different scan rates (20, 40, 60, 80, and 100 mV s^{-1} along the direction of the arrow) of (A) CP, (B) Fe(0.03)-HCl(0.05)-CP-3, (C) Fe(0.03)-HCl(0.05)-CP-9, and (D) Fe(0.03)-HCl(0.00)-CP-9.

Table S1. Summaries of various operation parameters of modification, the corresponding modified conditions, and the pH values of the system.

sample code	Concentration (mol/L)		Temperature (K)	pH value
	$FeCl_3$	HCl		
Fe(0.03)-H(0.00)-CP	0.03	0.00	333	2.04
Fe(0.03)-H(0.02)-CP	0.03	0.02	333	1.66
Fe(0.03)-H(0.03)-CP	0.03	0.03	333	1.50
Fe(0.03)-H(0.04)-CP	0.03	0.04	333	1.38
Fe(0.03)-H(0.05)-CP	0.03	0.05	333	1.31
Fe(0.03)-H(0.06)-CP	0.03	0.06	333	1.25
Fe(0.03)-H(0.07)-CP	0.03	0.07	333	1.18
Fe(0.03)-H(0.08)-CP	0.03	0.08	333	1.12
Fe(0.03)-H(0.09)-CP	0.03	0.09	333	1.04
Fe(0.03)-H(0.10)-CP	0.03	0.10	333	0.98
Fe(0.06)-H(0.00)-CP	0.06	0.00	333	1.85
Fe(0.06)-H(0.04)-CP	0.06	0.04	333	1.32
Fe(0.06)-H(0.05)-CP	0.06	0.05	333	1.26
Fe(0.06)-H(0.06)-CP	0.06	0.06	333	1.18
Fe(0.06)-H(0.07)-CP	0.06	0.07	333	1.13
Fe(0.06)-H(0.08)-CP	0.06	0.08	333	1.09
Fe(0.06)-H(0.09)-CP	0.06	0.09	333	1.03
Fe(0.06)-H(0.10)-CP	0.06	0.10	333	1.01
Fe(0.06)-H(0.11)-CP	0.06	0.11	333	0.96
Fe(0.06)-H(0.12)-CP	0.06	0.12	333	0.92

Table S2. Compositions of CP, Fe(0.03)-H(0.05)-CP-9 and Fe(0.03)-H(0.00)-CP-9 obtained via EDX quantitative analysis.

	Fe at.%	O at.%	Si at.%	Al at.%	Na at.%	K at.%
CP	0.00	63.90	28.51	6.52	1.07	5.05
Fe(0.03)-H(0.05)-CP-9	0.55	62.95	30.26	6.19	0.00	0.00
Fe(0.03)-H(0.00)-CP-9	9.57	60.97	23.10	6.34	0.00	0.00

Table S3. Summary of textural properties for various samples

Sample	BET surface area ($m^2 \cdot g^{-1}$)	Micropore surface area ($m^2 \cdot g^{-1}$)	External surface area ($m^2 \cdot g^{-1}$)	Micropore Volume ($mL \cdot g^{-1}$)
CP	28.749	4.274	24.476	0.003
Fe(0.03)-H(0.05)-CP-3	33.364	10.111	23.253	0.005
Fe(0.03)-H(0.05)-CP-9	34.921	12.081	22.840	0.006
Fe(0.03)-H(0.00)-CP-9	67.003	40.670	26.333	0.018

Table S4. Summaries for $\Delta_r G^{\theta}_m$ (kJ/mol), $\Delta_r S^{\theta}_m$ (J/mol k), $\Delta_r H^{\theta}_m$ (kJ/mol), and E_a (kJ) values of various modified process with NH_4-CP.

Samples	Exchange Times	298K		313K		333K		$\Delta_r H^{\theta}_m$	E_a
		$\Delta_r G^{\theta}_m$	$\Delta_r S^{\theta}_m$	$\Delta_r G^{\theta}_m$	$\Delta_r S^{\theta}_m$	$\Delta_r G^{\theta}_m$	$\Delta_r S^{\theta}_m$		
Fe(0.06)-H(0.07)-CP-x	1	-4.67	2.47	-4.92	2.47	-5.32	2.47	2.75	7.45
	3	-4.42	1.89	-4.65	1.97	-4.89	2.05	1.27	9.28
	5	-4.39	1.93	-4.60	2.00	-4.96	2.12	1.41	10.96
	7	-4.42	1.92	-4.63	1.99	-4.91	2.09	1.35	15.89
	9	-4.34	1.92	-4.52	1.98	-4.79	2.07	1.42	17.12
Fe(0.06)-H(0.07)-CP-x	1	-3.51	2.36	-3.72	2.43	-4.02	2.53	3.58	8.78
	3	-3.27	2.12	-3.46	2.18	-3.76	2.29	3.09	13.87
	5	-3.16	2.06	-3.42	2.15	-3.65	2.23	3.02	18.49
	7	-3.05	1.47	-3.25	1.54	-3.56	1.64	1.35	22.95

Table S5. Summaries of overpotentials (η) at 10 mA cm^{-2} and tafel slopes in 1.0 M KOH solution for OER properties obtained in this work and reported literature.

catalysts	η (mV)	Tafel slope (mV dec^{-1})	Reference
Fe(0.03)-H(0.05)-CP-9	560	129	this work
Fe(0.03)-H(0.00)-CP-9	510	79	this work
commercial RuO_2	330	76.3	[1]
$Co_{0.89}Fe_{0.11}O$-N	304	52.7	[1]
MIL-53(Fe)	233	88.7	[2]
CoNiFe ZIF-NFs	273	87	[3]
Fe-Co-CN/rGO	308	138	[4]
FeO_xCF-8	408	93	[5]
$CoFe_2O_4$/biocarbon	417	--	[6]

References

[1] Du, Q.; Su, P.; Cao, Z.; Yang, J.; Price, C.; Liu, J. Construction of N and Fe co-doped CoO/Co_xN interface for excellent OER performance. *Catal. Sci. Technol.* **2021**, 10.1016/j.susmat.2021.e00293.

[2] Nivetha, R.; Kollu, P.; Chandar, K.; Pitchaimuthu, S.; Jeong, S.; Grace, A. Role of MIL-53(Fe)/hydrated–dehydrated MOF catalyst for electrochemical hydrogen evolution reaction (HER) in alkaline medium and photocatalysis. *RSC advances* **2019**, *9*, 3215–3223.

[3] Sankar S.; Manjula K.; Keerthana G.; Babu B.; Kundu S. Highly stable trimetallic (Co, Ni, and Fe) zeolite imidazolate framework microfibers: an excellent electrocatalyst for water oxidation. *Cryst. Growth Des.* **2021**, *21*, 1800–1809.

[4] Fang W.; Wang J.; Hu Y.; Cui Q.; Zhu R.; Zhang Y.; Yue C.; Dang J.; Cui W.; Zhao H.; Li Z. Metal-organic framework derived Fe-Co-CN/reduced graphene oxide for efficient HER and OER. *Electrochim. Acta.* **2021**, *365*, 10.1021/acsami.7b08647.

[5] Yan F.; Zhu C.; Wang S.; Zhao Y.; Zhang X.; Chen Y. Electrochemically activated-iron oxide nanosheet arrays on carbon fiber cloth as a three-dimensional self-supported electrode for efficient water oxidation. *J. Mater. Chem. A*. **2016**, *4*, 6048–6055.

[6] Liu S.; Bian W.; Yang Z.; Tian J.; Jin C.; Shen M.; Zhou Z.; Yang R. A facile synthesis of CoFe2O4/biocarbon nanocomposites as efficient bi-functional electrocatalysts for the oxygen reduction and oxygen evolution reaction. *J. Mater. Chem. A.* **2014**, *2*, 18012–18017.